Commercial-Scale Visible-light Trifluoromethylation of 2-Chlorothiophenol using CF_3I gas.

Kaid C. Harper*[†], En-xuan Zhang*[‡], Zhi-qing Liu[‡], Timothy Grieme[†], Timothy Towne[†], Daniel Mack[†], Jeremy Griffin[†], Song-yuan Zheng[‡], Ning-ning Zhang[‡], Srinivas Gangula[‡], Jia-long Yuan[‡], Robert Miller[†], Ping-zhong Huang[‡], James Gage[‡], Moiz Diwan[†], Yi-Yin Ku[†]

* Correspondence to Kaid C. Harper (kaid.harper@abbvie.com), En-xuan Zhang (zhangenxuan@asymchem.com.cn)

† Abbvie Process R&D 1401 N. Sheridan Road, North Chicago, IL

‡ Asymchem Laboratories (Tianjin) Co. Ltd., TEDA, Tianjin 300457, P. R. China

Abstract:

Despite the growth of photoredox methods in academia, application of photoredox at scale in the pharmaceutical and fine chemical industries has been slow. In this report, a photoredox trifluoromethylation of a thiophenol was modified from the original literature report and the mechanism was investigated to define key scale-up parameters. The mechanistic insight was leveraged in the design and execution of two different reactor designs: an LED-based plug flow photoreactor as well as a laser-based continuous stirred tank photoreactor. In one of the first examples of commercial scale photoredox chemistry, the process was scaled to provide over 500 kilograms of the desired intermediate and amended to fully continuous manufacturing.

Manuscript:

The use of photochemistry can transform the way that active pharmaceutical ingredients are manufactured.[1-4] The last decade has seen widespread publication of new visible light-mediated transformations. Medicinal chemistry quickly adapted and applied these transformations, and their use has become common.[5-8] However, uptake of these new methodologies in process chemistry has lagged due to significant challenges associated with scaling light sources and related limitations of the Beer-Lambert law.[9] Despite these challenges, the appeal of the photochemical-based transformations remains undeniable and industrial commitments to green chemistry and efficient processing demanded a functional solution. Since 2017 AbbVie and Asymchem have made separate investments into understanding the scale up principles of photochemical reactions in flow, resulting in successes in scale-up in both the UV and visible regions of the spectrum, but the examples were limited in scale and scope.[10-13] Herein, we describe a partnered effort between Asymchem and AbbVie to scale up a visible-light mediated trifluoromethylation of 2-chlorothiophenol (**1**) which led to the successful synthesis of over 500 kgs of desired product (**2**) in high yield and purity and overall improved process efficiency and economics. This work represents the first commercial use of photoredox chemistry in pharmaceutical or fine chemical industries.

Previous efforts at the synthesis of trifluoromethyl product **2** made use of super-stoichiometric amounts of CF_3 transfer reagents but suffered from low to moderate yields. Noel and coworkers reported the photochemical trifluoromethylation of simple thiophenols using a $Ru(Bipy)_3Cl_2$ photocatalyst and CF_3I

gas, which is a desirable reagent for scale-up of trifluoromethylation.[14] Using the literature conditions and **1** with a small laboratory laser as the light source, we observed complete conversion to **2** within 20 seconds. The results of this initial experiment provided **2** in better than 96% crude purity. The reaction conditions were modified slightly to improve the manufacturability of the process and make use of bench stable sources of CF_3I.[15] Particularly, using tetramethylguanidine (TMG) as the base simplified the byproduct removal and amenability to scale. Initial lab-based results made use of commercially available TMG-CF_3I complex; however, larger scale reactions required dissolution of CF_3I gas into acetonitrile in the presence of TMG (vide infra). Adjusting the photocatalyst concentration to ensure optical saturation provided consistent results between scales of 100 mg to 10 grams (1 cm to 5 cm path lengths). The final reaction conditions used for scale-up are shown in Figure 1.

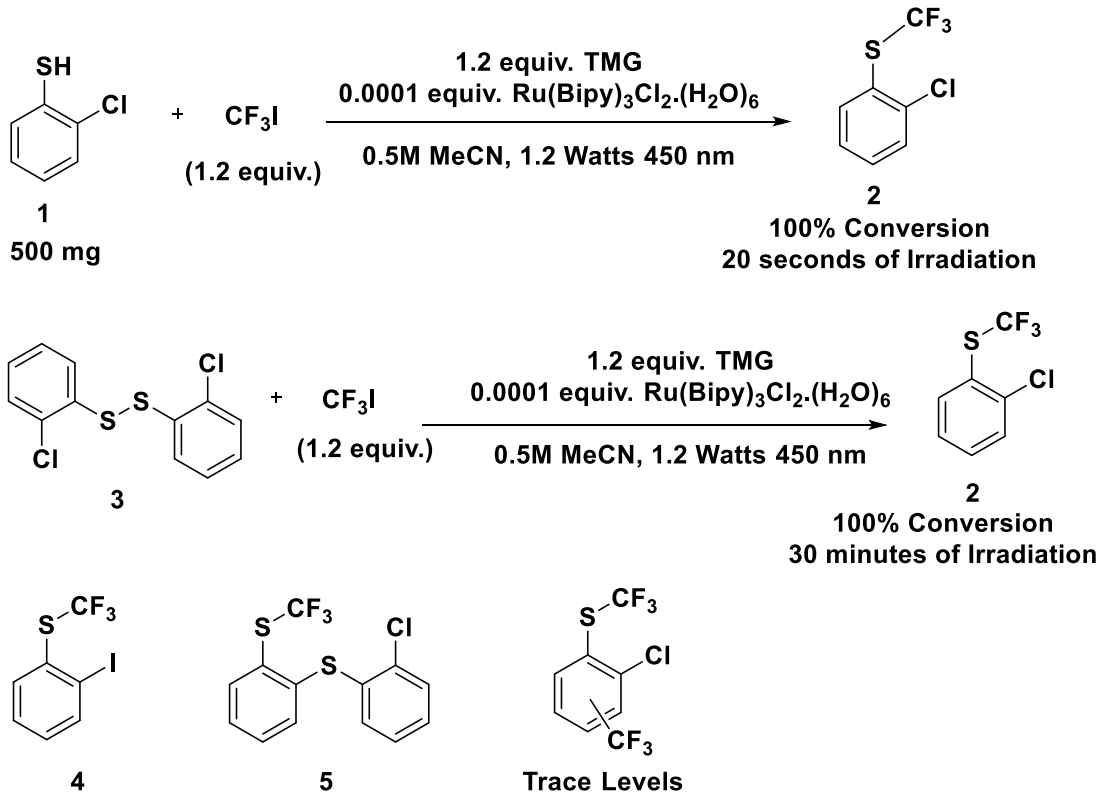

Figure 1. Optimized reaction conditions for the trifluoromethylation of thiophenol **1**, and the observed reactivity of disulfide **3** and key impurities formed in the reaction.

The accelerated timelines of the parent project necessitated quick determination of the reaction impurities to ensure the new photochemical route would not impact the downstream purity profile. The three primary byproducts identified were the disulfide (**3**), iodo-substituted byproduct (**4**) and a dimeric byproduct (**5**). Byproduct **5** had not been observed via other routes of synthesis and little was known of its downstream reactivity, therefore, controlling the amount of **5** became a key consideration as the reactor configuration was optimized. Disulfide **3** was identified as an impurity in the starting material at variable amounts; however, Noel *et al*. reported that disulfides were viable substrates to the

trifluoromethylation reaction. Hence, **3** was also evaluated as a potential starting material in the reaction and was found to be active albeit at rates 100X slower than **1**.

Having identified suitable reaction conditions and the nominal impurity profile, we turned our attention to understanding the reaction mechanism to better enable application of the optimal reactor design. Scaling a photochemical reaction has traditionally been challenging because it requires understanding and control of the photon flux as well as understanding how that surface irradiation translates across an absorption gradient. Indeed, the two most important design criteria for photoflow reactors are the effective quantum yield of the reaction and the molar extinction of the photocatalyst, both parameters of the photon flux. The molar extinction coefficient of $[Ru(Bipy)_3]Cl_2$ is known in the literature to be 14600 $M^{-1}cm^{-1}$ at 450 nm.[16, 17] Studying the reaction using a precise laser under batch conditions, the effective quantum yield was determined to be 92 ± 5.[18] A quantum yield of greater than 1 is typically interpreted as possessing a radical chain component with greater numbers indicating increasing prevalence of the radical chain mechanism over the photoredox mechanism.[19-23] For the trifluoromethylation reaction, the observed high quantum yield essentially indicates the reaction is catalytic in photons. Noel and coworkers proposed a reaction mechanism in their report; however, they did not address the radical chain component of the reaction. To account for the observed quantum yield and the use of a non-redox active base, the hybrid mechanism in Figure 2 was proposed.[24] The reaction initiates via absorption of a blue photon by the photocatalyst. The excited photocatalyst is quenched reductively by the thiolate anion producing a thiyl radical species **7** through which intersect several mechanisms. The productive radical chain pathway proceeds via alkylation of the thiyl radical by CF_3I which in turn generates iodine radical. The iodine radical then acts as an oxidative quenching species in the photoredox cycles and as a propagating radical in the chain reaction. Comparing these two reaction potentials according to literature reports of their potentials against SCE, the quench of the photocatalyst is more favorable with a ΔG of electron transfer (ΔG_{ET}) of -1.68 V;[25] whereas iodine radical oxidation of **6** to **7** is estimated at ΔG_{ET} of -0.03.[26] This suggests that the reductive quench is considerably more favorable; however, based on the relative concentrations of the photocatalyst and the thiolate anion (1000:1 at the beginning of the reaction), it is reasonable to propose that iodine can play both roles. Chain termination could occur via two pathways: Iodine oxidation of the photocatalyst and the homodimerization of **7** to form disulfide **3**. Disulfide **3** is competent to undergo alkylation under the reaction conditions but must operate via an energy transfer mechanism and not photoredox. This mechanism provides a basis for the strong radical chain component observed is supported by the impurity profile of the reaction under the nominal conditions where **4** was observed at higher levels (0.8-1.0%) than dimeric byproduct **5** (0.3-0.5% for **5**) and only trace amounts of the radical trifluoromethyl addition to the aryl ring were observed, indicating elevated concentrations of iodine radical over thiyl radical to form radical S_NAr impurities.[27,28-30] Control experiments were conducted to confirm the necessity of the blue light, and no reactivity was observed in the absence of light. Similarly, attempts to initiate the radical chain via radical initiation reagents all failed, indicating the radical chain was best sustained via continual generation of a small concentration of thiyl radical **7** under mild conditions.[31-33] In other words, the photoredox cycle is uniquely suited to sustain the radical chain. This mechanistic understanding provided a foundation upon which different flow reactors were built which

met the reaction requirement for photon flux but were also engineered to control other reaction variables such as temperature and residence time.

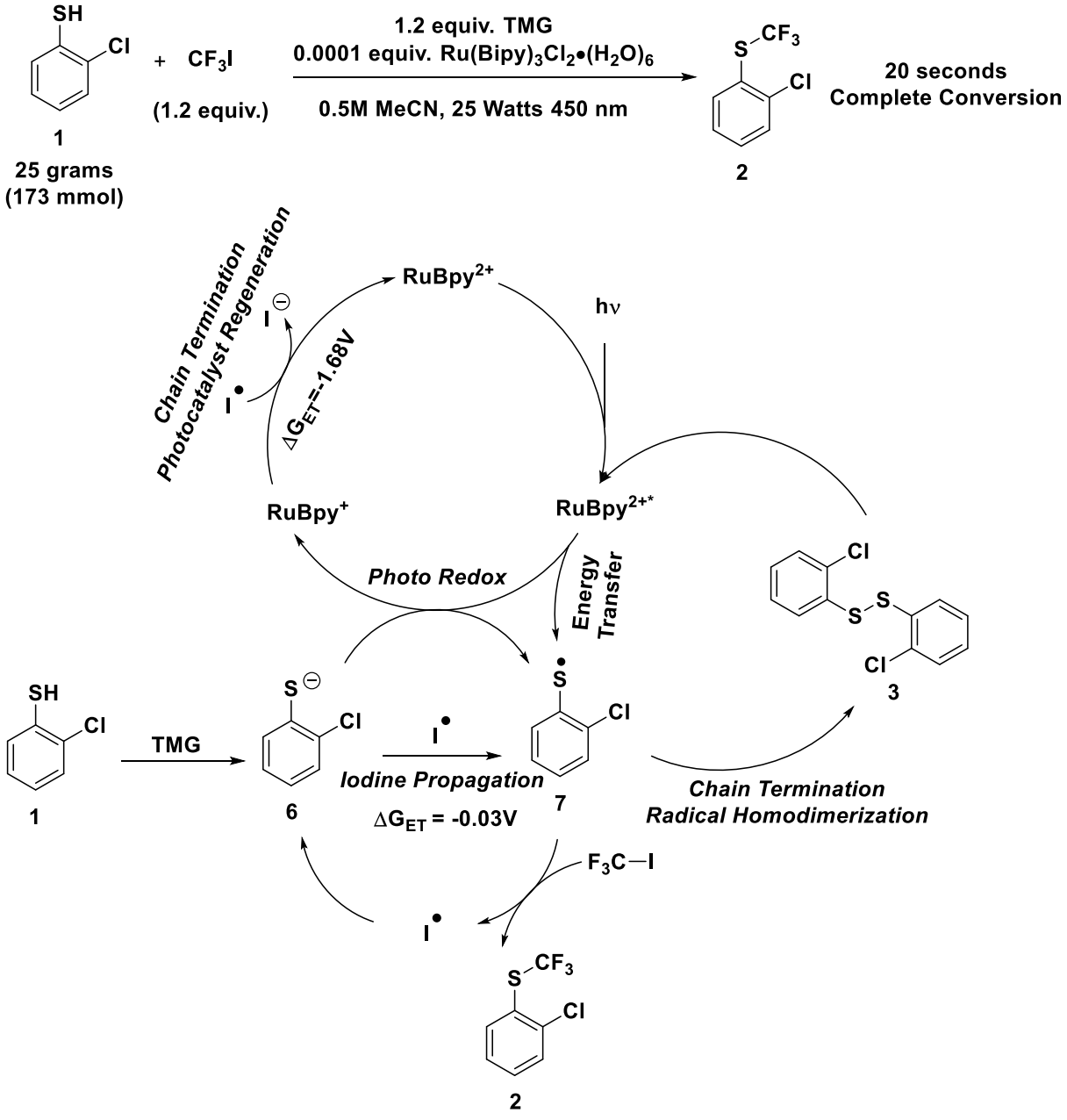

Figure 2. Proposed photoredox and radical chain mechanisms.

Leveraging the understanding of the reaction mechanism, AbbVie Process R&D partnered with Asymchem Inc. in an iterative process of design and implementation of photoflow reactors. In

collaboration, initial reactor options were explored for scale-up of the process to generate multiple 100+ kg batches of **2**. While the reaction had been optimized using laser-based reactor configurations, laser equipment was not available to Asymchem within the desired timeframe (1-2 months) so efforts were directed towards scaling the reaction using LEDs as the light source in conjunction with a plug flow reactor (PFR). [34-37] Asymchem had previous success scaling similar reactors using UV LEDs [10, 11] and several different research groups have reported success using such reactions on scales up to 1 kg but greater scales were not known at the time but have been reported since. [34, 37]

After an LED-PFR system was selected, the focus became identifying stable feed solutions for the initial scale-up. A system which combined the photocatalyst and thiophenol **1** in a feed and TMG and CF_3I in another feed met the criteria of being stable over long periods of time, gave consistent reaction performance, and was amenable to the available processing equipment. Other combinations of reagents did not provide the necessary stability. Further studies of the thiophenol **1** and photocatalyst solution demonstrate stability in excess of 14 days. Focused studies of the CF_3I and TMG solution stability yielded interesting results. Due to low boiling point of CF_3I (-20 ^oC), loss of potency of the solution during the projected 100-hour processing time was a concern. TMG had been initially selected as the desired base due to the bench stable complex it forms with CF_3I as reported by Ritter *et al*. and because it can be readily removed during the workup via mild acidic washes.[15] The feed solution of TMG and CF_3I was studied using IR spectroscopy with the hope that TMG would stabilize the gas and to prevent loss of potency in the feed solution at ambient temperatures. No such stabilization was observed as is shown in Figure 3A. In fact, a solution of CF_3I without TMG exhibited superior stability. Based on the results in Figure 3A, the TMG-CF_3I solution was held at or below temperatures of -5 to 0 ^oC to ensure adequate stability.

Once the feed solutions were identified and suitable stability was demonstrated, the light source/reactor configuration was addressed. Asymchem possessed a bank of 600 W (total output) 450 nm LEDs arrayed in a grid which was identified as an adequate light source for scale-up. Because overreaction or photobleaching was not observed, the primary reactor concern was control of the temperature due to the exothermicity of the reaction.[38] The scale-up reactor was constructed of 10 mm OD PFA tubing placed on average 1 cm from the LEDs. The light power was adjusted to provide a calculated surface irradiation of 15.5 mW/cm^2. To facilitate less material intensive studies a lab-scale PFR was also constructed of 3.2 mm OD PFA tubing and irradiated with 30 LEDs at 25 mW maximum output power. The output power of the LEDs was then adjusted to provide similar irradiation intensity (15.5 mW/cm^2) as the scale-up unit. Translating results between scales has been a long-standing challenge in photochemistry due to variability in the light sources.[9] Using consistent irradiation intensity between scales and a sufficiently low photocatalyst loading (to minimize variation based due to light absorption/transmission) consistent results between scales should have been obtained. However, Figure 3B summarizes the preliminary experiments comparing the lab-scale and scale-up reactors where higher levels of the impurity **5** were observed in the scale-up equipment and no clear steady state control of the reactor was demonstrated. This was alarming and warranted further investigations into the primary cause of the discrepancy between scales.

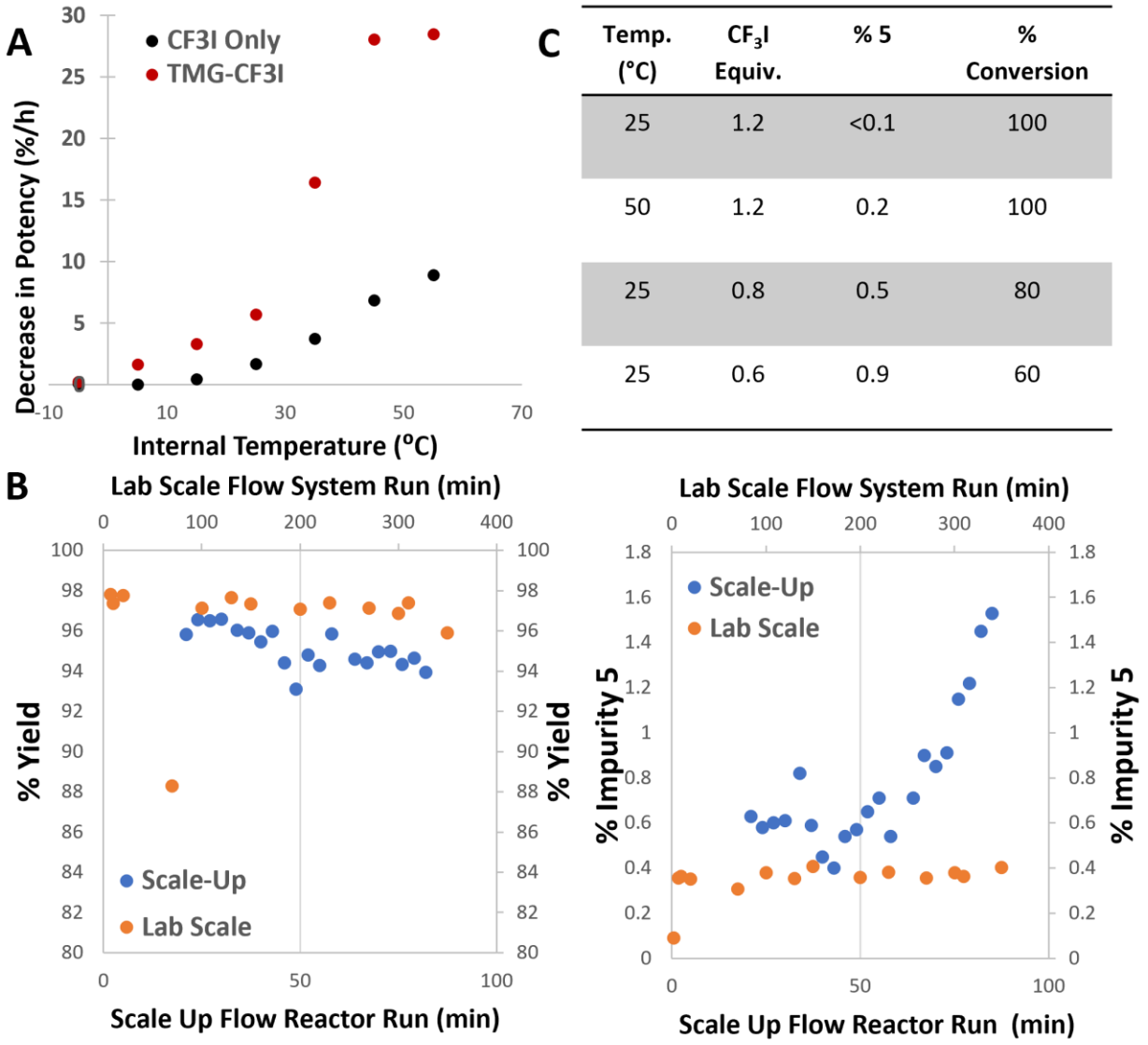

C

Temp. (°C)	CF_3I Equiv.	% 5	% Conversion
25	1.2	<0.1	100
50	1.2	0.2	100
25	0.8	0.5	80
25	0.6	0.9	60

Figure 3. A. Stability of CF_3I solutions in the absence and presence of TMG. **B**. Comparison of scale-up and lab-scale PFRs demonstrating a lack of control of impurity **5** upon scale-up. **C.** Experimental conditions which impacted formation of Impurity **5**.

Immediately, temperature variation between the scales was suspected as a likely cause of the inconsistency. Measurement of the outlet temperature from the flow reactor at steady state was 45-50 °C, despite cooling the feed solution temperatures to 0 °C while the lab-scale reactor outlet temperature was 25-30 °C with similar feed temperatures. During the flow reaction, the enclosed chamber surrounding the LEDs and PFR in the scale-up reactor warmed slowly overtime to temperatures in excess of 50 °C. No such warming occurred in the lab scale unit. To evaluate the effect of temperature on the flow reactor, the lab scale reactor was evaluated at several different temperatures via a controlled recirculating water bath. The results shown in Figure 4B revealed that higher levels of impurity **5** could be partially attributed to overheating in the reactor. Controlling reaction temperature

is a significant challenge associated with LED-based reactors.[9, 37] Due to the diffusive nature of LED sources, the PFR must be placed in close proximity to the LEDs themselves to ensure high photon flux. However, high powered LEDs produce a considerable amount of heat which must be decoupled from the reactor, creating a need for two close proximity temperature-controlled zones.[39] Temperature control in similar PFRs has been reported by several groups by submersing the reactor into recirculating bath making use of waterproof LEDs.[34, 37] However, available equipment was not amendable to this approach. Instead, indirect temperature control of the PFR was exerted by controlling and monitoring the feed solution temperatures.

Temperature variation did not completely account for the high levels of impurity **5** observed in the initial scale-up. Lab evaluations in flow which varied the flowrate of feed solutions, effectively decreasing the ratio of CF_3I to **1**, revealed that the impurity formation was indeed very sensitive to stoichiometry as shown in Figure 3C. This observation further supports the proposed mechanism, where in the absence of iodine radical to propagate the desired reaction, greater amounts of thiyl radical are formed and react via the S_NAr pathway to form **5**. Based on this data, it was concluded that pumping of the scale-up unit was susceptible to pulsation which in turn contributed to the higher levels of impurity **5**. To eliminate pulsation on scale-up, pulse dampeners and double diaphragm pumps were employed to minimize flowrate variation in the PFR.

Ultimately, the key reaction parameters of temperature, stoichiometry, and photon flux were harmonized between scales provided confidence for the scale-up. The execution of the flow scale-up was performed with run times between 80 and 100 hours and with 70-85 kg batches of 2-chlorothiophenol. The schematic in Figure 4A pictorializes how the reaction was executed. The feed solutions were delivered to the processing floor from remote temperature-controlled tanks and pumped into the reactor via smaller holding tanks. The solutions were pumped through heat exchanging equipment to arrive at feed solution temperatures which averaged -10 ^oC at the point of mixing. The reaction mixture then proceeded into the plug flow reactor residence loops totaling 400 mL of irradiated volume with a target 2-minute residence time. The 2-minute residence time was employed to manage reaction exothermicity and allow for adequate heat dissipation. The performance of the flow reactor over time is shown in Figure 4C for the six batches manufactured using this route. The outlet temperature was recorded over time and varied between 17.5 ^oC and 19.5 ^oC over all 6 runs demonstrating that the reaction temperature could be adequately controlled via temperature of the feed solutions. The collected material showed full conversion and 96% assay yield, impurity **5** was held to an acceptable level of ~0.5% and the overall yield after workup ranged between 85-92% giving a throughput of 20 kg/day.

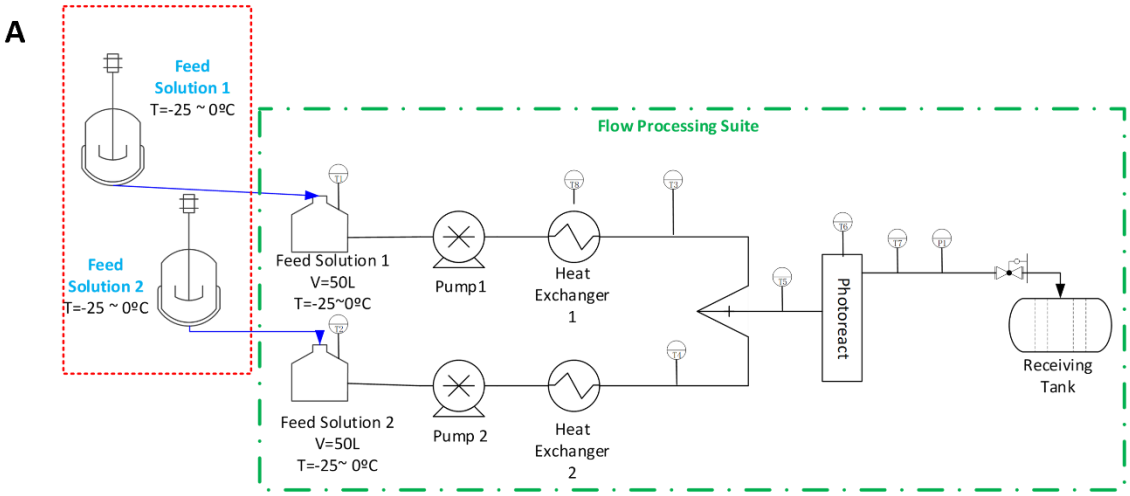

B

Run #	Amount of 1	% Yield
1	70	86
2	75	92
3	85	87
4	70	85
5	70	87
6	70	86

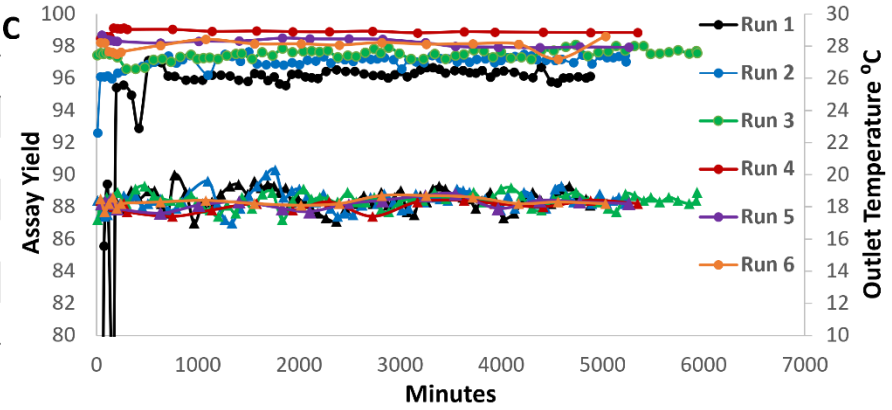

Figure 4. A. Process flow schematic for the photoflow using an LED-PFR reactor. **B.** Final results of the six runs executed in the reactor system. **C.** Assay yield and temperature performance of each run with assay yield on the left X-axis and data represented with dots and reactor outlet temperature on the right X-axis with triangles.

Our efforts in scaling the plug flow reactor highlighted several challenges that had been foreseen for scaling this type of reactor, namely controlling reactor temperature in the presence of high intensity irradiation from LEDs. To overcome each of these challenges, a fiber-coupled laser was substituted as the light source with a continuous stirred tank reactor (CSTR) as the flow reactor. Using this setup, the reaction could be actively and controllably cooled using a jacketed CSTR reactor and chiller in place of the indirect temperature control of the LED-PFR. While we have previously explored the laser CSTR as means of delivering higher intensity light to a smaller reactor footprint, in this case, the main advantage of using a fiber-coupled laser was the segregation of the heat associated with light generation from the reactor itself, allowing for greater temperature control. Also, a back-mixed CSTR would provide a mixing buffer against flowrate fluctuation, limiting the formation of impurity **5**. By exploiting the advantages of CSTR flow platform, the reaction residence time could be decreased to 60 seconds and the reactor volume increased, effectively quadrupling the throughput.

Additionally, the excellent efficiency of the photoflow reaction provided an opportunity to apply flow chemistry and continuous processing to the downstream synthesis of key intermediate **8**. When successfully applied, continuous manufacturing provides numerous benefits to fine chemical and pharmaceutical manufacturing including improved throughput, energy efficiency and flexibility.[40-42] The existing synthesis of **8** called for batch oxidation of intermediate **2** using sodium periodate in the presence of a ruthenium catalyst. While the reaction performed well in batch, the workup required six washes and a filtration to remove salts prior to final distillation. To render the synthesis of **8** fully continuous, homogeneous oxidation conditions were required as well as continuous workups for both reactions.

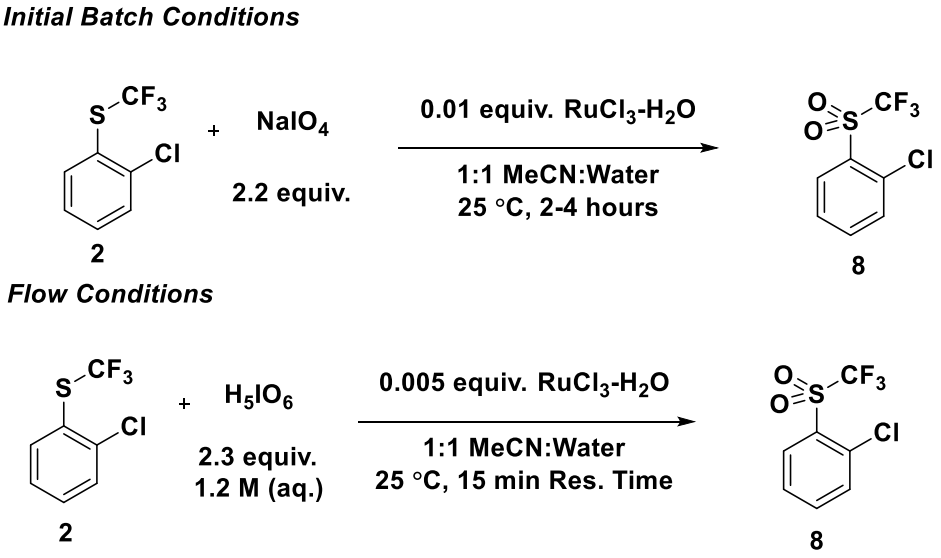

Figure 5. Batch and flow oxidation conditions.

The initial oxidation reaction conditions are shown in Figure 5 which used sodium periodate as the stoichiometric oxidant. The reaction concentration is below the solubility of sodium periodate which does not completely dissolve resulting in a triphasic reaction with a solid phase and two liquid phases a saturated sodium periodate solution and an organic phase containing hydrophobic **2**. Rather than pursue a cumbersome engineering solution to render such a reaction amenable to continuous manufacturing, different oxidants were explored which would eliminate the presence of solids. Substituting periodic acid for sodium periodate resulted in a rapid biphasic reaction (aqueous and organic). Different rates of reaction were observed when different stirring rates were employed, indicating the reaction was mixing sensitive. Because of the mixing sensitivity, a CSTR was identified as the optimal reactor platform. The stability of the ruthenium catalyst was impacted by the ratio of water to acetonitrile with 1:1 ratio being optimal. The feed solutions for this oxidation were evaluated next. The feed solution originating from the upstream photoflow reaction required dilution to provide the identified optimal solvent ratio. Evaluation of the other reagents revealed that combining the $RuCl_3$ and periodic acid led to precipitation and inconsistent performance, so the two reagents were dosed separately into the CSTR. An optimal residence time was identified at 15 minutes sufficient to provide 99% conversion and 96% product purity.

Having rendered both reactions amenable to continuous manufacturing, we turned our attention to the workup of the photoreaction. In this case, the aqueous washes were rendered continuous through the application of contiguous mixer settlers with two 5 wt % monobasic potassium phosphate washes, in a direct translation of the batch conditions. Contiguous washes were required to limit the amount of residual TMG to below 0.15 wt% to ensure a consistent purity profile in the subsequent oxidation. Batch evaluation of the washes showed 4-6% yield loss. Because of the acceptable yield loss to the wash cycles, little effort was extended to optimizing the workup conditions beyond a target 7-minute residence time in the mixer and a 20-minute residence time in the settler.

Optimization of the oxidation work-up conditions found that implementing a single wash of 10 wt% sodium meta-bisulfite eliminated many of the issues observed with the more elaborate workup and again could be implemented via a simple mixer-settler apparatus. Again, minimal optimization was performed around the residence times of the mixer-settler with a 5-minute mixing time and a 13-minute settling time empirically observed to be sufficient.

To demonstrate the advantages of the fully continuous manufacture over the mixed flow-batch process, each individual unit operation was demonstrated at kilogram scale separately, demonstrating that 50 kg/day throughput was achievable.[43] As a final proof-of-concept, the fully continuous reactor train was assembled using available lab space and equipment as shown in Figure 6. To fit the fully continuous process into the limited fume hood space, ¼ commercial scale equipment for the oxidation and workup sequence. The fully continuous demonstration was limited to 300 grams; enough to achieve a reasonable steady-state evaluation and successfully demonstrate the viability of the fully continuous process. Using the laser CSTR an average of 99.7% conversion was achieved, with 0.2% of impurity **5** observed. Steady state levels of TMG were observed at 0.13% after the continuous workup. In the oxidation, at steady state an average of 99.97% conversion was observed and following the workup a stream of 98.8% crude product purity was observed, an improvement of 1% compared to the original process. Assay yield for the continuous process at steady state averaged 85.3%, an improvement of 8% compared to the original process. Overall, application of continuous manufacturing to the process provided higher quality material and improved yield. We expect the application of a fully continuous process to increase the effective throughput by 4-10X, a testament to advantages of continuous manufacture in the pharmaceutical industry.

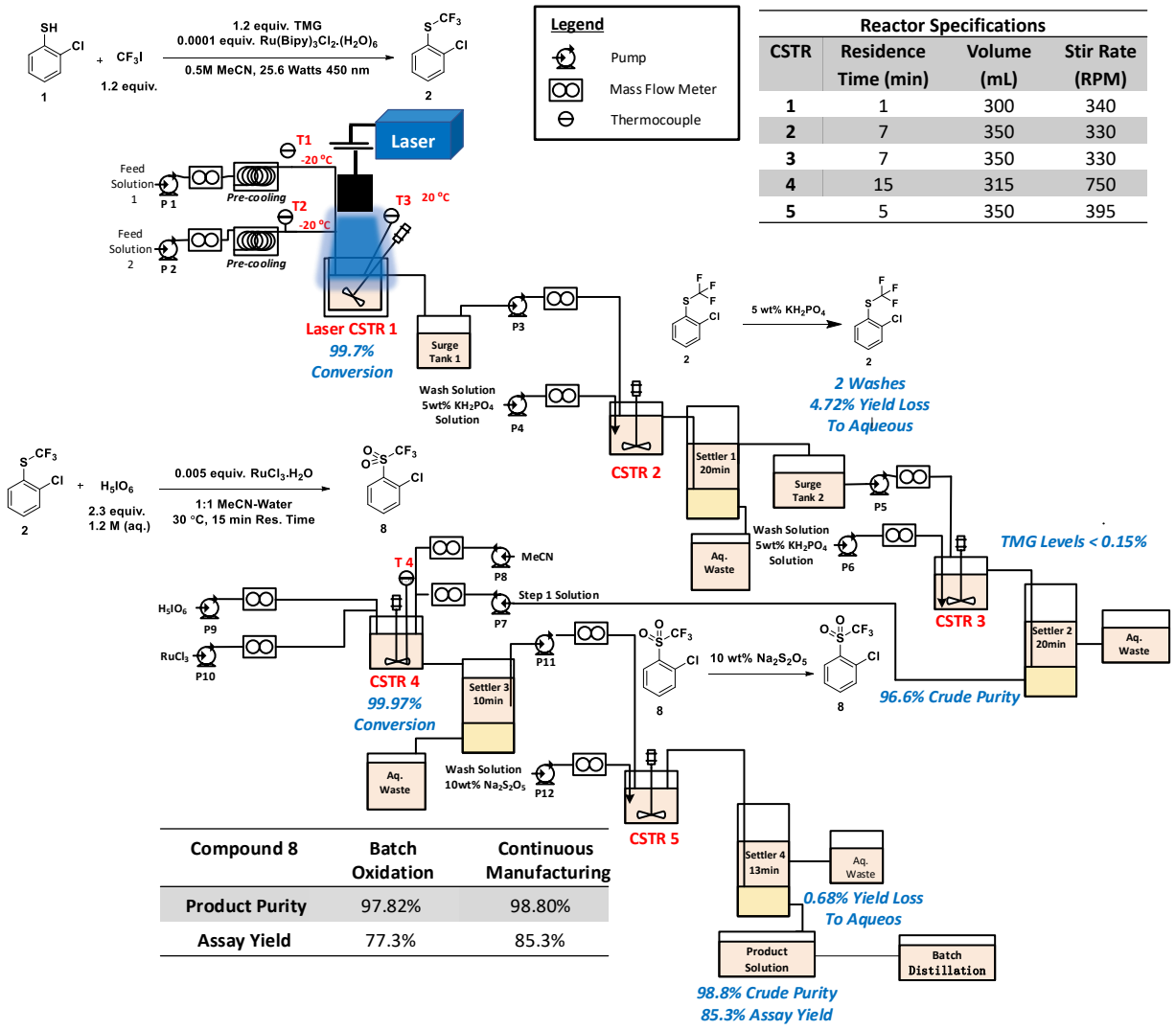

Reactor Specifications			
CSTR	Residence Time (min)	Volume (mL)	Stir Rate (RPM)
1	1	300	340
2	7	350	330
3	7	350	330
4	15	315	750
5	5	350	395

Compound 8	Batch Oxidation	Continuous Manufacturing
Product Purity	97.82%	98.80%
Assay Yield	77.3%	85.3%

Figure 6. Fully continuous manufacturing schematic employing a laser CSTR photoreactor, reaction work up and the continuous oxidation in a CSTR and work up.

Acknowledgement

Kaid Harper, Timothy Grieme, Timothy Towne, Daniel Mack, Jeremy Griffin, Robert Miller, Moiz Diwan and Yi-Yin Ku are employees of AbbVie and may own AbbVie stock. AbbVie sponsored and funded the study. AbbVie contributed to the design; participated in the collection, analysis, and interpretation of data, and in writing, reviewing, and approval of the final publication.

References

1. Shaw, M. H.; Twilton, J.; MacMillan, D. W. C., Photoredox Catalysis in Organic Chemistry. *The Journal of Organic Chemistry* **2016,** *81* (16), 6898-6926.
2. Romero, N. A.; Nicewicz, D. A., Organic Photoredox Catalysis. *Chemical Reviews* **2016,** *116* (17), 10075-10166.

3. McAtee, R. C.; McClain, E. J.; Stephenson, C. R. J., Illuminating Photoredox Catalysis. *Trends in Chemistry* **2019,** *1* (1), 111-125.
4. 20 Photocatalysis in the Pharmaceutical Industry. In *Photocatalysis in Organic Synthesis*, Georg Thieme Verlag: Stuttgart, 2019.
5. Boström, J.; Brown, D. G.; Young, R. J.; Keserü, G. M., Expanding the medicinal chemistry synthetic toolbox. *Nature Reviews Drug Discovery* **2018,** *17* (10), 709-727.
6. Zhang, R.; Li, G.; Wismer, M.; Vachal, P.; Colletti, S. L.; Shi, Z.-C., Profiling and Application of Photoredox C(sp3)–C(sp2) Cross-Coupling in Medicinal Chemistry. *ACS Medicinal Chemistry Letters* **2018,** *9* (7), 773-777.
7. Borlinghaus, N.; Kaschel, J.; Klee, J.; Haller, V.; Schetterl, J.; Heitz, S.; Lindner, T.; Dietrich, J. D.; Braje, W. M.; Jolit, A., Reagent and Catalyst Capsules: A Chemical Delivery System for Reaction Screening and Parallel Synthesis. *The Journal of Organic Chemistry* **2021,** *86* (2), 1357-1370.
8. Bogdan, A. R.; Gesmundo, N. J.; Webster, M. P.; Wang, Y.; Vasudevan, A., Recent Advances in Chemistry Technologies and Applications to Medicinal Chemistry. In *Burger's Medicinal Chemistry and Drug Discovery*, pp 1-78.
9. Bonfield, H. E.; Knauber, T.; Lévesque, F.; Moschetta, E. G.; Susanne, F.; Edwards, L. J., Photons as a 21st century reagent. *Nature Communications* **2020,** *11* (1), 804.
10. Beaver, M. G.; Zhang, E.-x.; Liu, Z.-q.; Zheng, S.-y.; Wang, B.; Lu, J.-p.; Tao, J.; Gonzalez, M.; Jones, S.; Tedrow, J. S., Development and Execution of a Production-Scale Continuous [2 + 2] Photocycloaddition. *Organic Process Research & Development* **2020,** *24* (10), 2139-2146.
11. Graham, M. A.; Noonan, G.; Cherryman, J. H.; Douglas, J. J.; Gonzalez, M.; Jackson, L. V.; Leslie, K.; Liu, Z.-q.; McKinney, D.; Munday, R. H.; Parsons, C. D.; Whittaker, D. T. E.; Zhang, E.-x.; Zhang, J.-w., Development and Proof of Concept for a Large-Scale Photoredox Additive-Free Minisci Reaction. *Organic Process Research & Development* **2021,** *25* (1), 57-67.
12. Harper, K. C.; Moschetta, E. G.; Bordawekar, S. V.; Wittenberger, S. J., A Laser Driven Flow Chemistry Platform for Scaling Photochemical Reactions with Visible Light. *ACS Central Science* **2019,** *5* (1), 109-115.
13. Moschetta, E. G.; Richter, S. M.; Wittenberger, S. J., Heuristics, Protocol, and Considerations for Flow Chemistry in Photoredox Catalysis. *ChemPhotoChem* **2017,** *1* (12), 539-543.
14. Straathof, N. J. W.; Tegelbeckers, B. J. P.; Hessel, V.; Wang, X.; Noël, T., A mild and fast photocatalytic trifluoromethylation of thiols in batch and continuous-flow. *Chemical Science* **2014,** *5* (12), 4768-4773.
15. Sladojevich, F.; McNeill, E.; Börgel, J.; Zheng, S.-L.; Ritter, T., Condensed-Phase, Halogen-Bonded CF3I and C2F5I Adducts for Perfluoroalkylation Reactions. *Angewandte Chemie International Edition* **2015,** *54* (12), 3712-3716.
16. Vonlanthen, M.; Cevallos-Vallejo, A.; Aguilar-Ortíz, E.; Ruiu, A.; Porcu, P.; Rivera, E., Synthesis, characterization and photophysical studies of novel pyrene labeled ruthenium (II) trisbipyridine complex cored dendrimers. *Polymer* **2016,** *99*, 13-20.
17. Kalyanasundaram, K., Photophysics, photochemistry and solar energy conversion with tris(bipyridyl)ruthenium(II) and its analogues. *Coordination Chemistry Reviews* **1982,** *46*, 159-244.
18. See the SI for a definition and calculation of effective quantum yield.
19. Cismesia, M. A.; Yoon, T. P., Characterizing chain processes in visible light photoredox catalysis. *Chemical Science* **2015,** *6* (10), 5426-5434.
20. Qin, Y.; Zhu, Q.; Sun, R.; Ganley, J. M.; Knowles, R. R.; Nocera, D. G., Mechanistic Investigation and Optimization of Photoredox Anti-Markovnikov Hydroamination. *Journal of the American Chemical Society* **2021,** *143* (27), 10232-10242.

21. Yayla, H. G.; Peng, F.; Mangion, I. K.; McLaughlin, M.; Campeau, L.-C.; Davies, I. W.; DiRocco, D. A.; Knowles, R. R., Discovery and mechanistic study of a photocatalytic indoline dehydrogenation for the synthesis of elbasvir. *Chemical Science* **2016,** *7* (3), 2066-2073.
22. Kim, S.; Toste, F. D., Mechanism of Photoredox-Initiated C–C and C–N Bond Formation by Arylation of IPrAu(I)–CF3 and IPrAu(I)–Succinimide. *Journal of the American Chemical Society* **2019,** *141* (10), 4308-4315.
23. Till, N. A.; Tian, L.; Dong, Z.; Scholes, G. D.; MacMillan, D. W. C., Mechanistic Analysis of Metallaphotoredox C–N Coupling: Photocatalysis Initiates and Perpetuates Ni(I)/Ni(III) Coupling Activity. *Journal of the American Chemical Society* **2020,** *142* (37), 15830-15841.
24. The mechanism proposed by Noel and coworkers relied on reductive quenching by the trialkylamine base, which was replaced with TMG which is present as a guanidinium salt and unlikely to reductively quench a photocatalyst.
25. Roth, H. G.; Romero, N. A.; Nicewicz, D. A., Experimental and Calculated Electrochemical Potentials of Common Organic Molecules for Applications to Single-Electron Redox Chemistry. *Synlett* **2016,** *27* (05), 714-723.
26. Larsen, A. G.; Holm, A. H.; Roberson, M.; Daasbjerg, K., Substituent Effects on the Oxidation and Reduction Potentials of Phenylthiyl Radicals in Acetonitrile. *Journal of the American Chemical Society* **2001,** *123* (8), 1723-1729.
27. This assumes a consistent radical substituion reaction mechanism between 4 and 5.
28. Rossi, R. A., Phenomenon of radical anion fragmentation in the course of aromatic SRN reactions. *Accounts of Chemical Research* **1982,** *15* (6), 164-170.
29. Arora, A.; Teegardin, K. A.; Weaver, J. D., Reductive Alkylation of 2-Bromoazoles via Photoinduced Electron Transfer: A Versatile Strategy to Csp2–Csp3 Coupled Products. *Organic Letters* **2015,** *17* (15), 3722-3725.
30. Bunnett, J. F.; Kim, J. K., Evidence for a radical mechanism of aromatic "nucleophilic" substitution. *Journal of the American Chemical Society* **1970,** *92* (25), 7463-7464.
31. Dialkyl Peroxides and Hydroperoxides. In *Handbook of Free Radical Initiators*, 2003; pp 61-127.
32. Azo Compounds. In *Handbook of Free Radical Initiators*, 2003; pp 303-358.
33. Compounds with Weak C□C, N□N, C□N, and N□O Bonds. In *Handbook of Free Radical Initiators*, 2003; pp 359-419.
34. Beatty, Joel W.; Douglas, James J.; Miller, R.; McAtee, Rory C.; Cole, Kevin P.; Stephenson, Corey R. J., Photochemical Perfluoroalkylation with Pyridine N-Oxides: Mechanistic Insights and Performance on a Kilogram Scale. *Chem* **2016,** *1* (3), 456-472.
35. Lee, D. S.; Sharabi, M.; Jefferson-Loveday, R.; Pickering, S. J.; Poliakoff, M.; George, M. W., Scalable Continuous Vortex Reactor for Gram to Kilo Scale for UV and Visible Photochemistry. *Organic Process Research & Development* **2020,** *24* (2), 201-206.
36. Corcoran, E. B.; McMullen, J. P.; Lévesque, F.; Wismer, M. K.; Naber, J. R., Photon Equivalents as a Parameter for Scaling Photoredox Reactions in Flow: Translation of Photocatalytic C−N Cross-Coupling from Lab Scale to Multikilogram Scale. *Angewandte Chemie International Edition* **2020,** *59* (29), 11964-11968.
37. Lévesque, F.; Di Maso, M. J.; Narsimhan, K.; Wismer, M. K.; Naber, J. R., Design of a Kilogram Scale, Plug Flow Photoreactor Enabled by High Power LEDs. *Organic Process Research & Development* **2020,** *24* (12), 2935-2940.
38. The adiabatic temperture rise of the only the alkylation reaction (not the acid-base reaction) was observed to be 17^{o}C.
39. The LED panel used in this example employed a cooling mechanism for the circuitry but still resulted in signficant external heating.

40. Burcham, C. L.; Florence, A. J.; Johnson, M. D., Continuous Manufacturing in Pharmaceutical Process Development and Manufacturing. *Annual Review of Chemical and Biomolecular Engineering* **2018,** *9* (1), 253-281.
41. Cole, K. P.; Groh, J. M.; Johnson, M. D.; Burcham, C. L.; Campbell, B. M.; Diseroad, W. D.; Heller, M. R.; Howell, J. R.; Kallman, N. J.; Koenig, T. M.; May, S. A.; Miller, R. D.; Mitchell, D.; Myers, D. P.; Myers, S. S.; Phillips, J. L.; Polster, C. S.; White, T. D.; Cashman, J.; Hurley, D.; Moylan, R.; Sheehan, P.; Spencer, R. D.; Desmond, K.; Desmond, P.; Gowran, O., Kilogram-scale prexasertib monolactate monohydrate synthesis under continuous-flow CGMP conditions. *Science* **2017,** *356* (6343), 1144-1150.
42. Rogers, L.; Jensen, K. F., Continuous manufacturing – the Green Chemistry promise? *Green Chemistry* **2019,** *21* (13), 3481-3498.
43. See the Supporting Information for schematics and performance details of each unit operation.